



Graphene Petal Foams with Hierarchical Micro- and Nano-Channels for Ultrafast Spontaneous and Continuous Oil Recovery

Journal:	<i>Journal of Materials Chemistry A</i>
Manuscript ID	TA-ART-01-2022-000019.R1
Article Type:	Paper
Date Submitted by the Author:	23-Apr-2022
Complete List of Authors:	Wu, Shiwen; The University of Texas at Dallas, Mechanical Engineering Tian, Siyu; The University of Texas at Dallas, Mechanical Engineering Jian, Ruda; The University of Texas at Dallas, Mechanical Engineering Wu, Ting-Nan; The University of Texas at Dallas Milazzo, Tye; University of Notre Dame Luo, Tengfei; University of Notre Dame, Aerospace and Mechanical Engineering Xiong, Guoping; The University of Texas at Dallas, Mechanical Engineering

1 **Graphene Petal Foams with Hierarchical Micro- and**
2 **Nano-Channels for Ultrafast Spontaneous and Continuous**
3 **Oil Recovery**

4 Shiwen Wu¹, Siyu Tian¹, Ruda Jian¹, Ting-Nan Wu¹, Tye David Milazzo², Tengfei Luo^{2,*}, Guoping Xiong^{1,*}

5
6 ¹. Department of Mechanical Engineering, The University of Texas at Dallas, Richardson, Texas 75080, USA

7 ². Department of Aerospace and Mechanical Engineering, University of Notre Dame, Notre Dame, Indiana 46556,

8 USA

9
10
11 * Corresponding authors: Tengfei Luo: tluo@nd.edu; Guoping Xiong: guoping.xiong@utdallas.edu

Abstract

Marine oil contamination remediation remains a worldwide challenge. Siphon action provides a spontaneous, continuous, low-cost and green route for oil recovery. However, it is still limited by the low oil recovery rate due to insufficient internal pathways for oil transport. In this paper, a graphene petal foam (GPF)-based oil skimmer is designed and fabricated by plasma-enhanced chemical vapor deposition (PECVD) for ultrafast self-pumping oil recovery from oil/water mixtures. The hierarchical structure, containing micro- and nano-channels formed by interconnected graphene networks and vertically aligned graphene petals (GPs), respectively, and micro-pores inherited from the 3D interconnected structure of Ni foam, provides multiple fast passages for oil transport. An oil recovery rate of $135.2 \text{ L m}^{-2} \text{ h}^{-1}$ is achieved in dark condition for such oil skimmers, while the value is increased to $318.8 \text{ L m}^{-2} \text{ h}^{-1}$ under a solar irradiation of 1 kW m^{-2} because of the excellent solar-heating effect of GPs. Quantitative analyses suggest that 68.8% of such a high oil recovery rate is contributed by the nano-channels and micro-pores, while 31.2% arises from the micro-channels. Our demonstrated GPF oil skimmers exhibit great promise for fast spontaneous and continuous oil contamination cleanup.

Keywords

Graphene petal foam | siphon effect | oil transport | solar-heating effect | hierarchical channels

1 Along with the booming development of oil industry, oil spill and leakage accidents during
2 offshore oil production or marine transportation have resulted in tremendous economic losses
3 and significant damage to the marine environment¹⁻³. Since the dissolution of oil in water as
4 well as spreading of oil slick strongly depends on time, rapid actions are required to separate
5 oil from the bulk water to avoid causing severe damage to the ecosystem once oil spills occur.
6 Physical absorption by porous materials with selective wettability (e.g., oleophilic and
7 hydrophobic surface properties) has become a promising method for oil spill cleanup⁴⁻⁶. For
8 example, polydimethylsiloxane-modified graphene nanoribbon aerogels were developed to
9 extract oil from oil/water mixtures⁴. Compared to other conventional methods (e.g., *in situ*
10 combustion⁷ and bioremediation⁸), physical absorption provides a green route to clean up oil
11 spill without introducing secondary contaminations. Nevertheless, post-treatments such as
12 pumping or squeezing are generally required to recycle the absorbed oil^{9, 10}, leading to
13 undesirable complex equipment costs, large energy consumption, and continuous human
14 intervention.

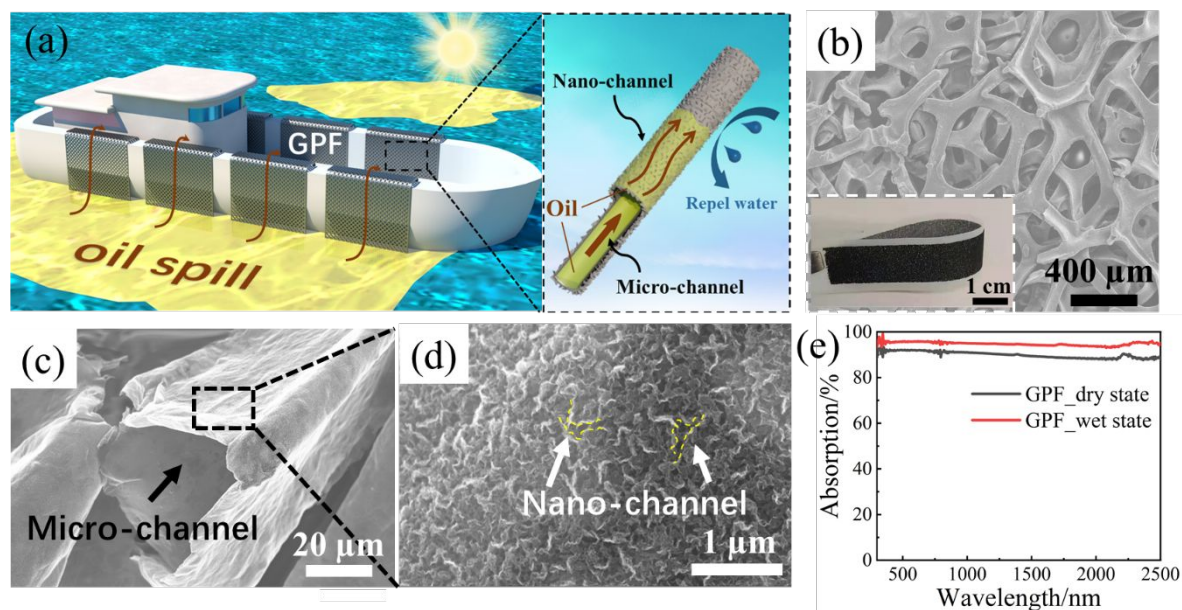
15 Recently, siphon effect, relying only on gravitational potential energy difference to
16 continuously transport liquids^{11, 12}, has been utilized for various applications such as irrigation,
17 oil recovery, and spillway¹³⁻¹⁸. As compared to conventional pump-assisted oil contamination
18 cleanup methods^{19, 20}, siphon action may provide a spontaneous, continuous, low-cost, and
19 green route with significantly reduced costs. However, low oil transport rate due to many
20 factors such as high viscosity of oil, and physical/chemical properties of channels restricts
21 further development of siphon-assisted oil recovery. To address the issue, light-absorbing
22 materials (e.g., carbon nanotubes²¹, MXene²²), which directly convert green solar energy to

1 thermal energy (i.e., photothermal effect), have been widely employed to reduce oil viscosity
2 and thus enhance oil transport rate²¹⁻²⁴. Combining siphon action with photothermal effect
3 provides an effective solution to improve the oil transport rate. In our prior work¹⁷, a siphon-
4 based oil skimmer equipped with surface-controlled nanochannels was designed to achieve
5 self-pumping oil recovery with a recovery rate of 35.2 L m⁻² h⁻¹ in dark condition, and the oil
6 recovery rate was increased to 123.3 L m⁻² h⁻¹ when exposed to solar irradiation of 1 kW m⁻².
7 Despite of the enhanced oil recovery rate, the oil recovery process still remains significantly
8 slower compared to conventional techniques relying on electricity-assisted pumping (e.g., over
9 500 L m⁻² h⁻¹)²⁵. Therefore, there is clearly room to further improve the oil recovery rate before
10 the wide-spread adoption of novel siphon oil skimmer strategy for practical applications.

11 Fluid transport through siphon effect is largely dependent on the properties of the internal
12 channels such as their density and structures^{26, 27}. Conventional oil recovery materials such as
13 melamine sponge^{28, 29} and graphene aerogels^{30, 31} mainly utilize their micro-sized pores for oil
14 transport and usually exhibit relatively low rates because of the insufficient number of internal
15 channels. Therefore, designing multiple transport pathways and rational channel structures are
16 required to achieve efficient siphon-assisted oil recovery. In our prior work, mechanically
17 robust graphene petal foams (GPF) with interconnected hollow internal channels exhibit
18 promising electrochemical performance due to the fast ionic transport properties in the
19 uniquely designed channels³². The combination of micro-sized hollow channels and the unique
20 nano-sized structure of graphene petals (GPs) leads to a significantly increased surface area
21 and corresponding outstanding electrical performance. Inspired by the unique structural design,
22 fast oil transport in graphene channels may be achieved by adopting such a unique hierarchical

1 structure with abundant micro- and nano-channels for multiple oil passages.

2 In this paper, we propose GPF oil skimmers with a uniquely designed hierarchical structure
3 containing micro- and nano-sized all-graphene channels for ultrafast spontaneous and
4 continuous oil recovery. As schematically illustrated in Figure 1a, free-standing GPF oil
5 skimmers in an inverted U-shape, consisting of vertically aligned GPs on the interconnected
6 three-dimensional (3D) graphene networks, are employed for siphon-assisted self-pumping oil
7 contamination cleanup. The nano-channels are formed by adjacent GPs grown vertically on the
8 Ni substrate through plasma-enhanced chemical vapor deposition (PECVD); and micro-
9 channels are formed by the hollow structure of the 3D graphene network, which is fabricated
10 by chemical etching of the Ni ligaments. Such hierarchical micro- and nano-sized all-graphene
11 channels can provide multiple pathways for efficient oil transport. Moreover, the oleophilic
12 and hydrophobic nature of graphene^{33, 34} ensures selectively oil transport from oil/water
13 mixtures. Together with the reduced oil viscosity resulting from the outstanding solar-heating
14 effect of GPs³⁵⁻³⁸, stable and efficient oil recovery rates up to 135.2 L m⁻² h⁻¹ and 318.8 L m⁻²
15 h⁻¹ are achieved in dark condition and under 1 sun of illumination (i.e., solar irradiance of 1
16 kW m⁻²), respectively, exhibiting great potential in practical applications such as marine oil
17 contamination cleanup without the need of electrical power.



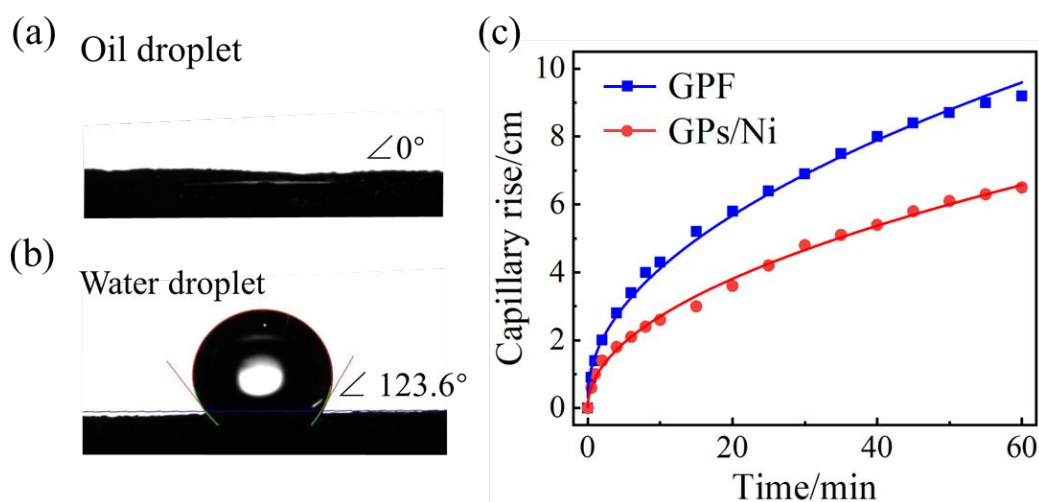
1
2 Figure 1. (a) Schematic illustration of GPFs with hierarchical micro- and nano-channels for efficient solar-
3 enhanced oil recovery. (b) SEM image of the GPF oil skimmer. Insert shows an optical image of the GPF oil
4 skimmer. SEM images of (c) micro-channels and (d) nano-channels in the GPF oil skimmer for oil transports.
5 (e) Absorption curves of the GPF oil skimmer within the solar spectrum under dry and wet states.

6 The GPF skimmers are prepared through a two-step process with details described in
7 Supplementary Materials. Briefly, GPs are firstly grown on the surface of compressed nickel
8 foams (Supplementary Figure S1) through PECVD. During the PECVD process, GPs with
9 widths ranging from approx. 100-500 nm are densely coated on Ni ligaments and perpendicular
10 to the Ni surface due to the influence of the plasma sheath near the substrate³⁹. The adjacent
11 vertically standing GPs on Ni ligaments can form nano-channels for oil transport. Subsequently,
12 Ni ligaments are etched by a facile chemical process³², leaving hollow micro-channels in free-
13 standing GPFs. Thus, the GPF skimmers with hierarchical micro- and nano-channels are
14 obtained to further enhance the transport pathways for ultrafast oil recovery. As shown in
15 Figure 1b, a typical GPF inherits the 3D interconnected structure of Ni ligaments and is highly

1 flexible on a thin Teflon film (inset in Figure 1b). Oil recovery tests with only Teflon film as
2 an oil skimmer are also conducted for comparison. Results show that no oil is collected after
3 48 hours (Supplementary Figure S2), indicating that the Teflon substrate exerts no influence
4 on the oil recovery process. The GPF skimmer with an inverted U-shape contains micro-
5 channels with a diameter of several tens of microns (Figure 1c) and nano-channels with a width
6 ranging from tens of nanometers to hundreds of nanometers (Figure 1d). Note that the vertically
7 standing GPs in GPFs show negligible structural changes during the etching of Ni foams
8 (Supplementary Figure S3), indicating the good chemical and mechanical stability of GPFs.
9 Moreover, the GPF skimmer exhibits high light absorption performance with an average
10 absorption of 90.0% in dry state and 94.8% when wetted by a mineral oil (Figure 1e), which
11 can be attributed to the light-trapped capability of the vertically aligned GPs (Supplementary
12 Figure S4)^{37, 38}. As such, solar energy can be efficiently absorbed and transformed to heat by
13 GPFs, which could potentially benefit oil transport by reducing its viscosity.

14 An ideal skimmer for selective oil transport from oil/water mixtures requires an oleophilic and
15 hydrophobic feature of the channel materials¹⁷. GPFs are composed of 3D graphene structures
16 which are naturally hydrophobic and oleophilic^{33, 34}. As shown in Figures 2a and 2b, oil
17 droplets can wet the GPF oil skimmer rapidly, while water droplets can stay on the surface of
18 the oil skimmer with a contact angle of 123.6°. The GPF oil skimmers can be treated to be
19 more hydrophobic through thermal reduction, with the water contact angle increased from
20 123.6° to 138.2° (Supplementary Figure S5a). Nonetheless, the performance of oil recovery
21 barely changes before and after the thermal reduction (Supplementary Figure S5b). Therefore,
22 we believe that the GPF oil skimmers without thermal reduction are sufficient to realize

1 effective oil recovery. We further characterize the capillary rise (h) of the mineral oil against
2 gravity as a function of time in GPF oil skimmers and compare the results with those of control
3 samples (i.e., GPs grown on Ni foams in which Ni ligaments are unetched, denoted as GPs/Ni),
4 as shown in Figure 2c. Supplementary Figure S6 shows the experimental setup, in which two
5 10-cm-height GPF and GPs/Ni samples are placed vertically, with one end immersed into
6 mineral oil and the other end fixed on a stand. The recorded data of capillary rises as a function
7 of time are fitted by Lucas-Washburn equation, which is widely used to describe capillary rise
8 behavior of liquids^{40, 41}. The GPF skimmer exhibits excellent oil-transport capability with an
9 oil capillary rise of 5 cm in 12 min because of the capillary forces arising from the micro- and
10 nano-channels. In contrast, it takes 30 min for oil to rise 5 cm in the GPs/Ni oil skimmer where
11 only nano-channels contribute to the capillary rise.



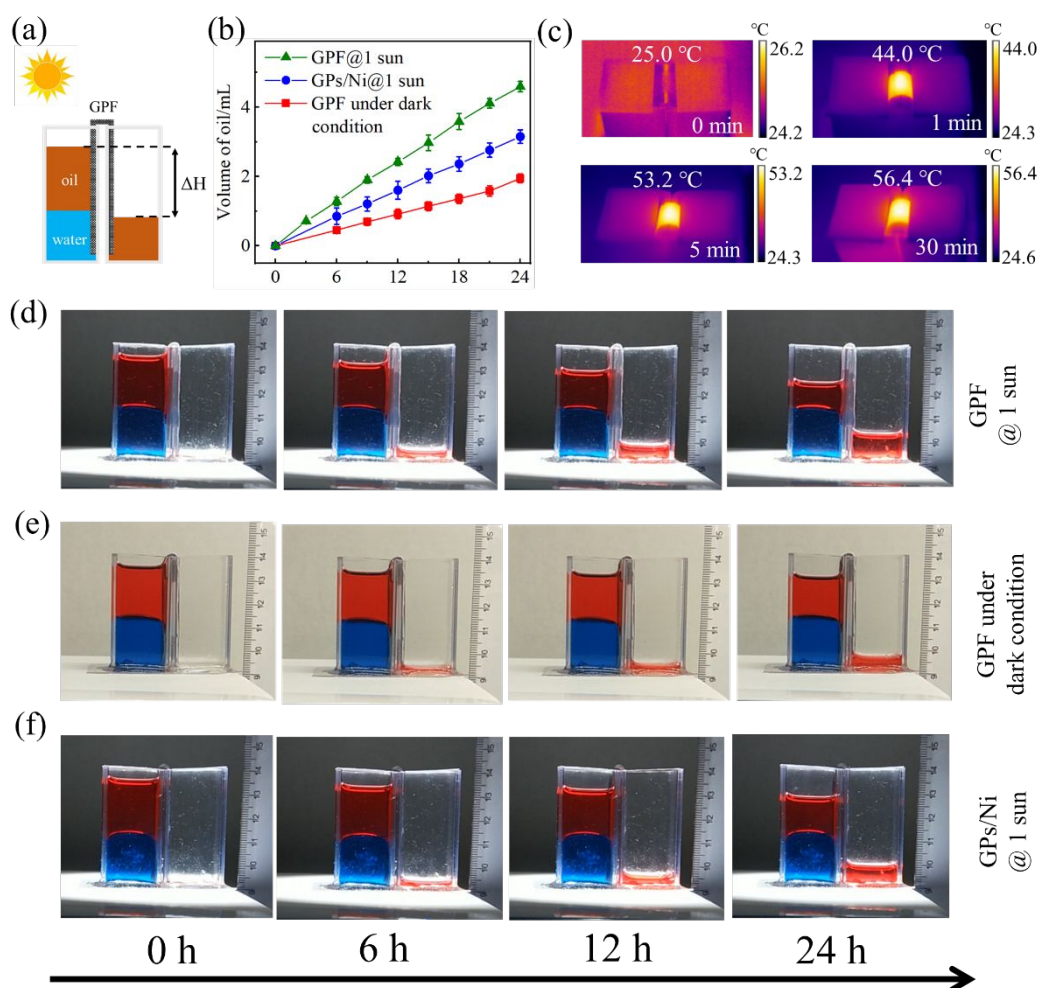
12

13 Figure 2. (a) Oil contact angle and (b) Water contact angle measurements of the GPF skimmer. (c) Capillary
14 rises of the mineral oil against gravity as a function of time in GPF and GPs/Ni oil skimmers.

15 Figure 3a exhibits a schematic of the experimental setup, containing two chambers separated
16 by a wall, for testing oil recovery. A mineral oil/water mixture with a volume ratio of 1:1 is

1 added to the left chamber to mimic the floating oil spilled on water, while the right chamber is
2 employed to collect and measure the content of the recovered oil transported from the left one.
3 The two chambers are connected by an inverted U-shape GPF or GPs/Ni oil skimmer, with the
4 height difference between the upper surfaces of oil in the left and right chambers (ΔH , indicated
5 in Figure 3a) fixed at 40 mm. The oil recovery tests are conducted both in dark condition and
6 under 1 sun of solar illumination. When exposed to the simulated sunlight, both chambers are
7 covered to ensure that only the top surface of oil skimmers are illuminated. As shown in Figure
8 3b, the volume of recovered oil by the GPF and GPs/Ni oil skimmers within 24 h are measured
9 by recording the processes using a digital camera (Supplementary Videos S1-2). Figures 3d-f
10 present snapshots of oil recovery processes by the GPF skimmers under 1 sun of solar
11 illumination and under dark condition, and by the GPs/Ni oil skimmers under 1 sun of solar
12 illumination. The GPF skimmer exhibits efficient oil transport performance with an average
13 oil recovery rate of $135.2 \text{ L m}^{-2} \text{ h}^{-1}$ in dark condition and $318.8 \text{ L m}^{-2} \text{ h}^{-1}$ under 1 sun of solar
14 illumination. The approximately 2.5-fold enhancement in oil transport rate of the GPF skimmer
15 under solar illumination can be primarily attributed to the decreased oil viscosity under solar
16 irradiation. Figure 3c shows the surface temperature evolution of the GPF oil skimmer under 1
17 sun of solar illumination. Due to the outstanding solar absorption properties of GPs, the
18 temperature of the top GPF surface rises quickly from ambient temperature (i.e., 25°C) to 53.2°C
19 within 5 min, and then reaches a stable value of approx. 56.2°C after 30 min. The increasing
20 surface temperature under solar irradiation leads to a decrease in oil viscosity, thereby
21 significantly enhancing the oil recovery rate (Figure 3b). The GPF oil skimmer exhibits
22 significant improvement of oil transport performance compared to our prior work¹⁷ (i.e.,

1 approximately 4-fold and 2.6-fold enhancements in dark condition and under 1 sun of solar
 2 illumination, respectively). A comparison of oil recovery rate between our work and other
 3 external power-driven oil recovery devices is shown in Supplementary Table S1.



4
 5 Figure 3. (a) Schematic illustration of the oil recovery setup. The blue color represents water. The red color
 6 represents mineral oil. Oil transports from the oil/water mixture in the left chamber to the right chamber
 7 through an inverted U-shape oil skimmer. ΔH represents the height difference between the upper surfaces of
 8 oil in the left and right chambers. (b) The volume evolutions of recovered oil by GPF and GPs/Ni under
 9 different conditions. (c) IR images exhibiting the surface temperature change of GPF working at 1 sun. (d)
 10 Optical images showing the oil recovery process by GPF at 1 sun. (e) Optical images showing the oil
 11 recovery process by GPF in dark condition. (f) Optical images showing the oil recovery process by GPs/Ni
 12 at 1 sun.

1 The hierarchical structure of the GPF skimmer provides three types of passages for oil transport:
2 nano-channels formed by GPs, micro-channels formed by the etching of Ni ligaments, and
3 micro-pores inherited from the 3D interconnected structure of Ni foam. The contribution of the
4 hollow micro-channels in GPF skimmers can be evaluated by comparing the oil transport rates
5 in GPF and GPs/Ni oil skimmers under 1 sun of solar illumination:

$$6 \quad v_m = \frac{\Delta V_{GPF} - \Delta V_{GPs/Ni}}{S\Delta t} \quad (1)$$

7 where ΔV_{GPF} and $\Delta V_{GPs/Ni}$ represent the volumes of transported oil during a period Δt through
8 the GPF and GPs/Ni oil skimmers under 1 sun, respectively. S represents the cross-sectional
9 area of the GPF oil skimmer which is 10 mm \times 0.06 mm (Supplementary Figure S7). From
10 Equation 1, the oil transport rate contributed by micro-channels in the GPF oil skimmers is
11 calculated to be 99.5 L m⁻² h⁻¹ (corresponding to 31.2% of the total oil transport rate). The rest
12 part of the oil transport rate (219.3 L m⁻² h⁻¹, corresponding to 68.8% of the total oil transport
13 rate) can be attributed to contributions from the nano-channels and micro-pores. In our prior
14 work, we showed that the morphology of GPs could be controlled by changing the growth time
15 during the PECVD process⁴². To investigate the effect of nano-channels on the oil recovery
16 process, GPF skimmers with different nano-channel structures are fabricated by setting the
17 growth time of GPs as 40, 80 and 120 min. SEM images in Supplementary Figure S8 show that
18 the GPs are grown more densely as the growth time increases, providing more nano-channels
19 with smaller channel widths for oil transport. The covered areas by GPs are also measured by
20 an open-source software (ImageJ), and the result shows that GPs are covering 16.6%, 24.1%,
21 and 33.0% of the surface of micro-channels as the PECVD growth durations are 40, 80, and

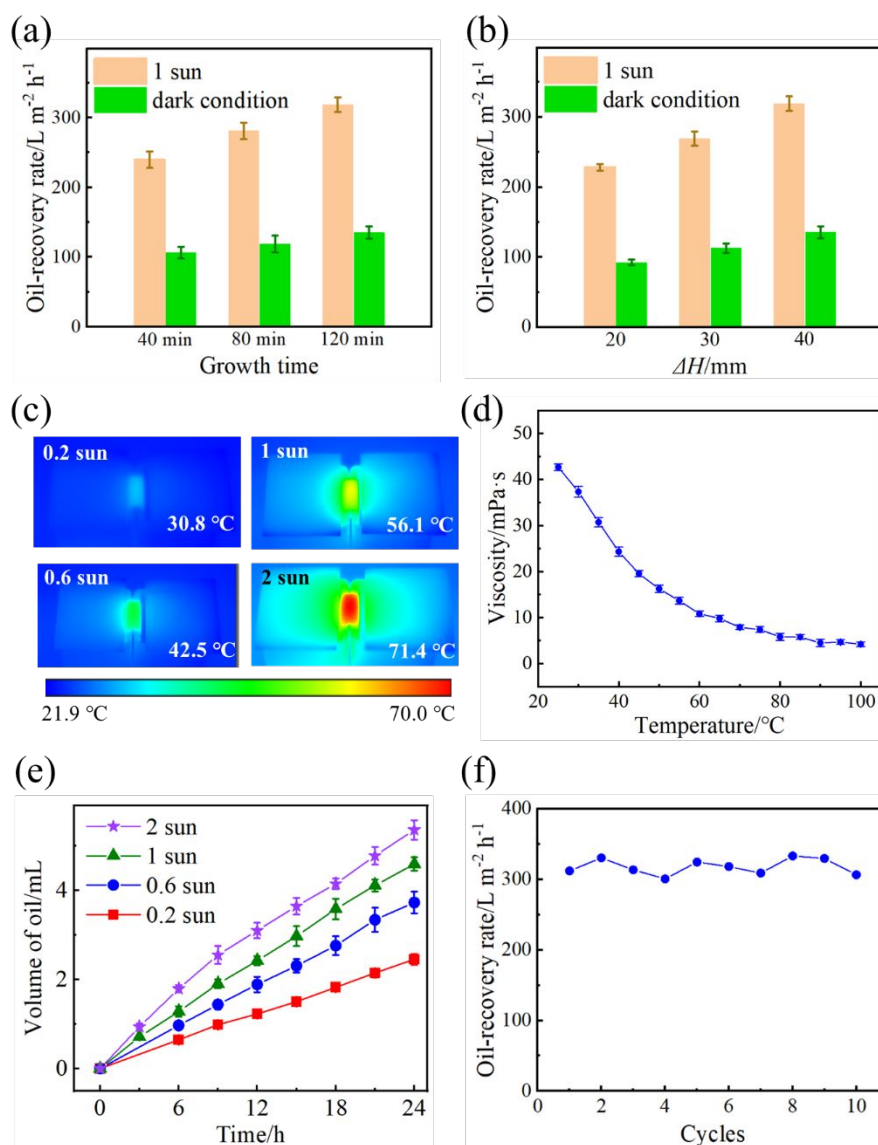
1 120 min, respectively. According to the Laplace-Young equation, a liquid inside a channel is
2 subjected to capillary force (F_c):⁴¹

$$3 \quad F_c = A \times \Delta P_c = A \times 2\sigma \cos\theta / r \quad (2)$$

4 where A is assumed to be the projected cross-sectional area of the transport channel, ΔP_c is
5 capillary pressure, σ represents the liquid surface tension, θ is the liquid-solid contact angle,
6 and r is the effective pore radius of the transporting channel. The capillary force on the liquid
7 increases as the channel size decreases. Consequently, higher oil recovery rates are achieved
8 in the oil skimmers with a longer growth time of GPs. As shown in Figure 4a, when the PECVD
9 growth time increases from 40 to 80 and 120 min, the average oil transport rate of the GPF
10 skimmers increases from 239.8 to 281.2 and 318.8 L m⁻² h⁻¹ under 1 sun and increases from
11 106.4 to 118.8 and 135.2 L m⁻² h⁻¹ in dark condition, respectively. We observe that further
12 decreasing the growth time (e.g., shorter than 40 min) of GPs leads to severe deterioration in
13 the mechanical properties, and structural collapses occur when the GP growth time is
14 excessively short. Therefore, quantitatively determining the contributions from the nano-
15 channels and micro-pores seems rather difficult.

16 Since siphon action is driven by the change of gravitational potential energy¹², the height
17 difference between the upper surfaces of oil in the left and right chambers (i.e., ΔH) largely
18 affects the oil recovery rate according to the Bernoulli's relation^{13, 17}. In this case, the effect of
19 ΔH on the oil recovery performance of GPF oil skimmers under dark condition and 1 sun of
20 illumination is investigated. As shown in Figure 4b, higher ΔH provides larger gravitational
21 potential energy differences (i.e., larger driving forces) for oil transport, leading to faster oil
22 recovery both under dark condition and at 1 sun. In addition, the intensity of solar irradiation

1 varies in practical applications. Therefore, systematical evaluation of the oil recovery
2 performance of the GPF skimmer under different solar irradiation intensities is highly
3 warranted. Thermal images of the GPF skimmer during oil recovery tests under different solar
4 irradiation intensities are recorded after solar illuminations for 30 min, as shown in Figure 4c.
5 The surface temperature of the GPF skimmer is promoted notably when the solar irradiation
6 intensity increases. Figure 4d shows that the viscosity of oil decreases rapidly as the
7 temperature increases. For example, the surface temperature of the GPF skimmer rises from
8 room temperature (i.e., 25°C) to 56°C when exposed to 1 sun of solar illumination, leading to a
9 reduction of 69.3% of the oil viscosity and thus a higher oil recovery rate. As shown in Figure
10 4e, the GPF oil skimmer exhibits average oil recovery rates of 135.2, 188.9, 244.9, 318.8, and
11 367.4 L m⁻² h⁻¹ at 0.2, 0.6, 1, and 2 suns of solar illumination, respectively.



1
 2 Figure 4. (a) Average oil transport rates of the GPF oil skimmers with different growth durations of GPs. (b)
 3 Comparison of the average oil transport rates of the GPF oil skimmer under different ΔH . (c) IR images
 4 exhibiting the surface temperatures of GPF oil skimmer working at 0.2, 0.6, 1, and 2 suns of illumination for
 5 30 min. (d) Viscosities of the mineral oil as a function of temperature. (e) Volume evolutions of recovered
 6 oil by GPF skimmers under different solar irradiation intensities. (f) Cyclic stability of the GPF skimmer.
 7 Tests are conducted under 1 sun with $\Delta H = 40$ mm.

8 In addition, cyclic stability of oil skimmers is another key factor that determines their overall
 9 performance in practical applications. We conduct a 10-cycle test (corresponding to 240 h in

1 total) on the oil recovery rate of the GPF oil skimmer under 1 sun, as shown in Figure 4f. The
2 oil recovery performance exhibits no noticeable degradation during the 240-h test, with the
3 recovery rate remains relatively stable between 300 and 330 L m⁻² h⁻¹, indicating the excellent
4 long-term cyclic stability of the GPF oil skimmer. Oil recovery tests based on another type of
5 oil (denoted as type 2 oil) with much higher viscosities are conducted on the GPF skimmer
6 (Supplementary Figure S9). Results show that the type 2 oil can also be recovered
7 spontaneously and continuously by the oil skimmer. An average oil recovery rate of 72.8 L m⁻²
8 h⁻¹ is achieved in dark condition, which can be further promoted to 168.0 L m⁻² h⁻¹ under 1
9 sun of solar illumination, indicating that the photothermal effect is also beneficial for
10 improving the oil transport performance of type 2 oil. Therefore, our proposed GPF oil
11 skimmers are capable to recover oil with a wide viscosity range.

12 In summary, ultrafast spontaneous and continuous oil recovery from oil/water mixtures is
13 achieved by the unique design of inverted U-shape GPF oil skimmers containing hierarchical
14 micro- and nano-channels. Because of the oleophilic and hydrophobic nature of graphene, GPF
15 oil skimmers show selective oil transport from oil/water mixtures. A typical GPF oil skimmer
16 exhibits a high oil recovery rate of 318.8 L m⁻² h⁻¹ under a solar irradiation of 1 kW m⁻², which
17 is 2.5-fold enhancement as compared to that (135.2 L m⁻² h⁻¹) in the dark condition because of
18 the solar-heating effect of GPs. The contributions from the hierarchical micro- and nano-
19 channels in the GPF skimmer are quantitatively analyzed by comparing the oil recovery
20 performance of the GPF with GPs/Ni oil skimmers. The results show that 68.8% of the oil
21 recovery rate is contributed by the nano-channels and the micro-pores inherited from the 3D
22 interconnected structure of Ni foam, while 31.2% is contributed by the micro-channels.

1 Moreover, the GPF oil skimmer exhibits long-term cyclic stability during a 240-h oil recovery
2 test. This work provides a novel strategy by combining the hierarchical micro- and nano-
3 channels to achieve fast oil transport without any external power input or assistance of
4 complicated devices, which can also be applied in separation of other liquid mixtures (e.g.,
5 water and other organic liquids). Further optimization of the growth conditions of GPs and
6 geometric parameters of Ni substrates can possibly further enhance the oil recovery rate of GPF
7 oil skimmers that is comparable or even than those of conventional pumping-based oil
8 skimmers.

9 **Supporting information**

- 10 1. Detailed information on materials, synthesis and characterization of GPF and GPs/Ni;
11 morphology of the compressed Ni foam; morphology of GPs before and after etching the
12 Ni substrate; schematic illustrating the light-trapped capability of GPs; thickness of the
13 GPF oil skimmer; comparison between the GPF oil skimmer and previous oil recovery
14 devices.
- 15 2. Accelerated (5000×) video of oil recovery by GPF under 1 sun
- 16 3. Accelerated (5000×) video of oil recovery by GPs/Ni under 1 sun
- 17 4. Accelerated (100×) video of capillary rise of the mineral oil against gravity on GPF
18 skimmer
- 19 5. Accelerated (100×) video of capillary rise of the mineral oil against gravity on GPs/Ni
20 skimmer

1 **Acknowledgements**

2 G.X. thanks the University of Texas at Dallas startup fund and the support from the NSF (Grant
3 No. CBET-1937949 and CBET-1949962). T.L. thanks the support from the NSF (Grant No.
4 CBET-1949910 and CBET-1937923). The authors thank Shilin You for the valuable
5 discussion and help during the preparation of the manuscript.

6 **Notes**

7 The authors declare no conflicts of interest.

8

9

References

1. Jernelöv, A., How to defend against future oil spills. *Nature* **2010**, *466* (7303), 182-183.
2. Ma, Q.; Cheng, H.; Fane, A. G.; Wang, R.; Zhang, H., Recent Development of Advanced Materials with Special Wettability for Selective Oil/Water Separation. *Small* **2016**, *12* (16), 2186-2202.
3. <https://www.cnn.com/2021/10/04/us/gallery/california-oil-spill-2021/index.html>.
4. Chen, L.; Du, R.; Zhang, J.; Yi, T., Density controlled oil uptake and beyond: from carbon nanotubes to graphene nanoribbon aerogels. *Journal of Materials Chemistry A* **2015**, *3* (41), 20547-20553.
5. Xue, Z.; Cao, Y.; Liu, N.; Feng, L.; Jiang, L., Special wettable materials for oil/water separation. *Journal of Materials Chemistry A* **2014**, *2* (8), 2445-2460.
6. Peng, M.; Zhu, Y.; Li, H.; He, K.; Zeng, G.; Chen, A.; Huang, Z.; Huang, T.; Yuan, L.; Chen, G., Synthesis and application of modified commercial sponges for oil-water separation. *Chemical Engineering Journal* **2019**, *373*, 213-226.
7. Ge, J.; Zhao, H.-Y.; Zhu, H.-W.; Huang, J.; Shi, L.-A.; Yu, S.-H., Advanced Sorbents for Oil-Spill Cleanup: Recent Advances and Future Perspectives. *Advanced Materials* **2016**, *28* (47), 10459-10490.
8. Pete, A. J.; Bharti, B.; Benton, M. G., Nano-enhanced Bioremediation for Oil Spills: A Review. *ACS ES&T Engineering* **2021**, *1* (6), 928-946.
9. Niu, H.; Li, J.; Wang, X.; Luo, F.; Qiang, Z.; Ren, J., Solar-Assisted, Fast, and In Situ Recovery of Crude Oil Spill by a Superhydrophobic and Photothermal Sponge. *ACS Applied Materials & Interfaces* **2021**, *13* (18), 21175-21185.
10. Zhang, R.; Wu, Y.; Zhang, H.; Xue, S.; Guo, M.; Zhang, T., A facile strategy toward hydrophobic-oleophilic 3D Fe foam for efficient oil-water separation. *Journal of Materials Science* **2019**, *54* (20), 13358-13367.
11. Boatwright, A.; Hughes, S.; Barry, J., The height limit of a siphon. *Scientific Reports* **2015**, *5* (1), 16790.
12. Hicks, J. W.; Badeer, H. S., Siphon mechanism in collapsible tubes: application to circulation of the giraffe head. *American Journal of Physiology-Regulatory, Integrative and Comparative Physiology* **1989**, *256* (2), R567-R571.
13. Jeong, G. S.; Oh, J.; Kim, S. B.; Dokmeci, M. R.; Bae, H.; Lee, S.-H.; Khademhosseini, A., Siphon-driven microfluidic passive pump with a yarn flow resistance controller. *Lab on a Chip* **2014**, *14* (21), 4213-4219.
14. Jin, J.; Zhao, X.; Du, Y.-H.; Ding, M.; Xiang, C.; Yan, N.; Jia, C.; Han, Z.; Sun, L., Nanostructured Three-Dimensional Percolative Channels for Separation of Oil-in-Water Emulsions. *iScience* **2018**, *6*, 289-298.
15. Sun, H.-y.; Wang, D.-f.; Shang, Y.-q.; Cai, Y.-l.; Wei, Z.-l., An improved siphon drainage method for slope stabilization. *Journal of Mountain Science* **2019**, *16* (3), 701-713.
16. Tadayon, R.; Ramamurthy, A. S., Discharge Coefficient for Siphon Spillways. *Journal of Irrigation and Drainage Engineering* **2013**, *139* (3), 267-270.
17. Wu, S.; Yang, H.; Xiong, G.; Tian, Y.; Gong, B.; Luo, T.; Fisher, T. S.; Yan, J.; Cen, K.; Bo, Z.; Ostrikov, K. K., Spill-SOS: Self-Pumping Siphon-Capillary Oil Recovery. *ACS Nano* **2019**, *13* (11), 13027-13036.
18. Zhang, Z.; Zhang, Y.; Fan, H.; Wang, Y.; Zhou, C.; Ren, F.; Wu, S.; Li, G.; Hu, Y.; Li, J.; Wu, D.; Chu, J., A Janus oil barrel with tapered microhole arrays for spontaneous high-flux spilled oil absorption and storage. *Nanoscale* **2017**, *9* (41), 15796-15803.
19. Ge, J.; Shi, L.-A.; Wang, Y.-C.; Zhao, H.-Y.; Yao, H.-B.; Zhu, Y.-B.; Zhang, Y.; Zhu, H.-W.; Wu, H.-A.; Yu, S.-H., Joule-heated graphene-wrapped sponge enables fast clean-up of viscous crude-oil spill. *Nature Nanotechnology* **2017**, *12* (5), 434-440.

- 1 20. Huang, Y.; Gancheva, T.; Favis, B. D.; Abidli, A.; Wang, J.; Park, C. B., Hydrophobic Porous Polypropylene
2 with Hierarchical Structures for Ultrafast and Highly Selective Oil/Water Separation. *ACS Applied Materials
3 & Interfaces* **2021**, *13* (14), 16859-16868.
- 4 21. Wu, X.; Lei, Y.; Li, S.; Huang, J.; Teng, L.; Chen, Z.; Lai, Y., Photothermal and Joule heating-assisted
5 thermal management sponge for efficient cleanup of highly viscous crude oil. *Journal of Hazardous
6 Materials* **2021**, *403*, 124090.
- 7 22. Ma, X.; Chen, K.; Li, S.; Gnanasekar, P.; Zhong, Y.; An, Y.; Luo, Q.; Huang, Q.; Zhu, J.; Chen, J.; Yan, N.,
8 Degradable Ti₃C₂T_x MXene Nanosheets Containing a Lignin Polyurethane Photothermal Foam (LPUF) for
9 Rapid Crude Oil Cleanup. *ACS Applied Nano Materials* **2022**, *5* (2), 2848-2858.
- 10 23. Chao, W.; Wang, S.; Li, Y.; Cao, G.; Zhao, Y.; Sun, X.; Wang, C.; Ho, S.-H., Natural sponge-like wood-
11 derived aerogel for solar-assisted adsorption and recovery of high-viscous crude oil. *Chemical Engineering
12 Journal* **2020**, *400*, 125865.
- 13 24. Li, Q.; Sun, Q.; Li, Y.; Wu, T.; Li, S.; Zhang, H.; Huang, F., Solar-Heating Crassula perforata-Structured
14 Superoleophilic CuO@CuS/PDMS Nanowire Arrays on Copper Foam for Fast Remediation of Viscous
15 Crude Oil Spill. *ACS Applied Materials & Interfaces* **2020**, *12* (17), 19476-19482.
- 16 25. He, S.; Cheng, X.; Li, Z.; Shi, X.; Yang, H.; Zhang, H., Green and facile synthesis of sponge-reinforced
17 silica aerogel and its pumping application for oil absorption. *Journal of Materials Science* **2016**, *51* (3),
18 1292-1301.
- 19 26. Narayanamurthy, V.; Jeroish, Z. E.; Bhuvaneshwari, K. S.; Bayat, P.; Premkumar, R.; Samsuri, F.; Yusoff,
20 M. M., Advances in passively driven microfluidics and lab-on-chip devices: a comprehensive literature
21 review and patent analysis. *RSC Advances* **2020**, *10* (20), 11652-11680.
- 22 27. Wang, P.; Yuan, S.; Yang, N.; Oppong, P. K., A comprehensive review on non-active micro-pumps for
23 microfluidic platforms. *Journal of Micromechanics and Microengineering* **2021**, *31* (9), 093001.
- 24 28. Stolz, A.; Le Floch, S.; Reinert, L.; Ramos, S. M. M.; Tuailon-Combes, J.; Soneda, Y.; Chaudet, P.; Baillis,
25 D.; Blanchard, N.; Duclaux, L.; San-Miguel, A., Melamine-derived carbon sponges for oil-water separation.
26 *Carbon* **2016**, *107*, 198-208.
- 27 29. Wang, C.-F.; Huang, H.-C.; Chen, L.-T., Protonated Melamine Sponge for Effective Oil/Water Separation.
28 *Scientific Reports* **2015**, *5* (1), 14294.
- 29 30. Xu, L.; Xiao, G.; Chen, C.; Li, R.; Mai, Y.; Sun, G.; Yan, D., Superhydrophobic and superoleophilic
30 graphene aerogel prepared by facile chemical reduction. *Journal of Materials Chemistry A* **2015**, *3* (14),
31 7498-7504.
- 32 31. Yang, S.; Shen, C.; Chen, L.; Wang, C.; Rana, M.; Lv, P., Vapor-Liquid Deposition Strategy To Prepare
33 Superhydrophobic and Superoleophilic Graphene Aerogel for Oil-Water Separation. *ACS Applied Nano
34 Materials* **2018**, *1* (2), 531-540.
- 35 32. Xiong, G.; He, P.; Wang, D.; Zhang, Q.; Chen, T.; Fisher, T. S., Hierarchical Ni-Co Hydroxide Petals on
36 Mechanically Robust Graphene Petal Foam for High-Energy Asymmetric Supercapacitors. *Advanced
37 Functional Materials* **2016**, *26* (30), 5460-5470.
- 38 33. Thakkar, S. V.; Pinna, A.; Carbonaro, C. M.; Malfatti, L.; Guardia, P.; Cabot, A.; Casula, M. F., Performance
39 of oil sorbents based on reduced graphene oxide-silica composite aerogels. *Journal of Environmental
40 Chemical Engineering* **2020**, *8* (1), 103632.
- 41 34. Wu, S.; Gong, B.; Yang, H.; Tian, Y.; Xu, C.; Guo, X.; Xiong, G.; Luo, T.; Yan, J.; Cen, K.; Bo, Z.; Ostrikov,
42 K. K.; Fisher, T. S., Plasma-Made Graphene Nanostructures with Molecularly Dispersed F and Na Sites for
43 Solar Desalination of Oil-Contaminated Seawater with Complete In-Water and In-Air Oil Rejection. *ACS
44 Applied Materials & Interfaces* **2020**, *12* (34), 38512-38521.

- 1 35. Tian, Y.; Yang, H.; Wu, S.; Yan, J.; Cen, K.; Luo, T.; Xiong, G.; Hou, Y.; Bo, Z.; Ostrikov, K., Beyond
2 lotus: Plasma nanostructuring enables efficient energy and water conversion and use. *Nano Energy* **2019**,
3 *66*, 104125.
- 4 36. Wu, S.; Xiong, G.; Yang, H.; Gong, B.; Tian, Y.; Xu, C.; Wang, Y.; Fisher, T.; Yan, J.; Cen, K.; Luo, T.;
5 Tu, X.; Bo, Z.; Ostrikov, K., Multifunctional Solar Waterways: Plasma-Enabled Self-Cleaning
6 Nanoarchitectures for Energy-Efficient Desalination. *Advanced Energy Materials* **2019**, *9* (30), 1901286.
- 7 37. Wu, S.; Xiong, G.; Yang, H.; Tian, Y.; Gong, B.; Wan, H.; Wang, Y.; Fisher, T. S.; Yan, J.; Cen, K.; Bo, Z.;
8 Ostrikov, K., Scalable Production of Integrated Graphene Nanoarchitectures for Ultrafast Solar-Thermal
9 Conversion and Vapor Generation. *Matter* **2019**, *1* (4), 1017-1032.
- 10 38. Xu, C.; Bo, Z.; Wu, S.; Wen, Z.; Chen, J.; Luo, T.; Lee, E.; Xiong, G.; Amal, R.; Wee, A. T. S.; Yan, J.;
11 Cen, K.; Fisher, T. S.; Ostrikov, K., Vertical graphene nano-antennas for solar-to-hydrogen energy
12 conversion. *Solar Energy* **2020**, *208*, 379-387.
- 13 39. Tian, S.; Wu, S.; Xiong, G., Graphitic nanopetals and their applications in electrochemical energy storage
14 and biosensing. *Journal of Nanoparticle Research* **2020**, *22* (5), 97.
- 15 40. Tsunazawa, Y.; Yokoyama, T.; Nishiyama, N., An experimental study on the rate and mechanism of
16 capillary rise in sandstone. *Progress in Earth and Planetary Science* **2016**, *3* (1), 8.
- 17 41. Cai, J.; Perfect, E.; Cheng, C.-L.; Hu, X., Generalized Modeling of Spontaneous Imbibition Based on Hagen-
18 Poiseuille Flow in Tortuous Capillaries with Variably Shaped Apertures. *Langmuir* **2014**, *30* (18), 5142-
19 5151.
- 20 42. Xiong, G.; Hembram, K. P. S. S.; Zakharov, D. N.; Reifenberger, R. G.; Fisher, T. S., Controlled thin
21 graphitic petal growth on oxidized silicon. *Diamond and Related Materials* **2012**, *27-28*, 1-9.

22